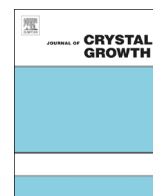




ELSEVIER

Contents lists available at ScienceDirect

Journal of Crystal Growth

journal homepage: www.elsevier.com/locate/jcrysgr

Lithium outdiffusion in LiTi_2O_4 thin films grown by pulsed laser deposition



S. Mesoraca*, J.E. Kleibeuker, B. Prasad, J.L. MacManus-Driscoll, M.G. Blamire

Department of Materials Science, University of Cambridge, 27 Charles Babbage Road, Cambridge CB3 0FS, United Kingdom

ARTICLE INFO

Article history:

Received 28 June 2016

Received in revised form

6 September 2016

Accepted 8 September 2016

Communicated by A. Ohtomo

Available online 9 September 2016

Keywords:

A3. Physical vapor deposition processes

B1. Oxides

B1. Lithium compounds

B1. Titanium compounds

B2. Oxide superconducting materials

ABSTRACT

We report surface chemical cation composition analysis of high quality superconducting LiTi_2O_4 thin films, grown epitaxially on MgAl_2O_4 (111) substrates by pulsed laser deposition. The superconducting transition temperature of the films was ~ 13.8 K.

Surface chemical composition is crucial for the formation of a good metal/insulator interface for integrating LiTi_2O_4 into full-oxide spin-filtering devices in order to minimize the formation of structural defects and increase the spin polarisation efficiency. In consideration of this, we report a detailed angle resolved x-ray photoelectron spectroscopy analysis. Results show Li segregation at the surface of LiTi_2O_4 films. We attribute this process due to outdiffusion of Li toward the outermost LiTi_2O_4 layers.

© 2016 The Authors. Published by Elsevier B.V. This is an open access article under the CC BY license (<http://creativecommons.org/licenses/by/4.0/>).

1. Introduction

In recent years, spin-filtering [1] has emerged as a promising way to polarise a charge current by means of a tunnel barrier with a ferromagnetic insulator (FI) and non-magnetic electrodes. Moreover, it has a theoretical capability to provide polarisation (P) up to $\sim 100\%$, rather than the limited 50% of conventional magnetic tunnel junctions with ferromagnetic electrodes [2]. The current polarisation occurs due to the difference in barrier heights for the two spin directions, created by the exchange splitting of the conduction band in the FI, at temperatures below the Curie temperature (T_{Curie}).

Spin-filter devices, working at low temperature, with high polarisation ($P=97\%$), have been studied extensively and are principally based on Eu-chalcogenide FIs with Curie temperature at the most 69 K [3–5] and GdN with a $T_{\text{Curie}}=30$ K [6]. With the attempt to obtain spin currents by spin-filtering at temperatures closer to room temperature, interest has also focused on tunnel junctions based on magnetic transition metal oxides, with higher magnetic ordering temperatures, like BiMnO_3 [7], $\text{Sm}_{0.75}\text{Sr}_{0.25}\text{MnO}_3$ [8,9] and $\text{Pr}_{0.8}\text{Ca}_{0.2}\text{Mn}_{1-y}\text{Co}_y\text{O}_3$ [10], but these devices showed spin polarisation only at cryogenic temperatures.

To achieve spin-filtering at a technologically useful temperature, one should consider spinel ferrites, such as CoFe_2O_4 , MnFe_2O_4 and NiFe_2O_4 . These oxides, although they have a complex crystal structure and high magnetic-electronic properties sensitivity to

structural and chemical defects, have T_{Curie} well above room temperature (~ 800 K) [11]. To date, a much lower than predicted polarisation ($P < 4\%$) has been demonstrated in CoFe_2O_4 based tunnel junctions at 290 K [12,13]. The likely reason being the formation of anti-phase boundaries (APBs) in the barrier [14,15] which are detrimental for spin-filter efficiency as they locally change magnetic behavior and barrier height. Such defects are formed due to spinel oxides having a lattice parameter ($a=0.8392\text{--}0.8511$ nm) [11] almost double of the metallic layers (Au, Pt, LaNiO_3 , $\text{La}_{2/3}\text{Sr}_{1/3}\text{MnO}_3$) and substrates conventionally used in spin-filter devices. Achieving high spin-filter efficiency at room temperature is therefore primarily dependent on eliminating structural and chemical defects in ultra-thin (< 5 nm) epitaxial spinel ferrites films to be used in complex oxide barriers.

To reduce defects, the metal-superconductor spinel oxide LiTi_2O_4 ($a=0.8405$ nm) [16], closely-lattice matched to spinel ferrites, could be used as non-magnetic electrodes in all-spinel spin-filter devices, grown on spinel MgAl_2O_4 ($a=0.8080$ nm) [17] substrates. As a result, an epitaxial system with near-perfect interfaces could be achieved, thus APBs and detrimental effects of interface anomalies on the polarisation of one or both the ferromagnetic layers should be minimized to greatly enhance the room temperature spin-filter efficiency.

Since the discovery of superconductivity by Johnston et al. [18] in 1973, LiTi_2O_4 triggered high interest as it was the first oxide superconductor with a relatively high critical temperature ($T_c=11$ K) and it was one of the very few ternary systems to exhibit an elevated critical temperature. LiTi_2O_4 belongs to the

* Corresponding author.

$\text{Li}_{1+x}\text{Ti}_{1-x}\text{O}_4$ ternary system, which also includes the electrical insulating $\text{Li}_{4/3}\text{Ti}_{5/3}\text{O}_4$ phase ($x=1/3$), i.e. for $x > 0$ a metal to insulator composition-induced transition occurs. Even though sample reproducibility and lack of high quality LiTi_2O_4 thin films are known issues [19–21] that have hampered the understanding of this spinel ternary system, there have been numerous studies on this unique spinel oxide. Recently, high quality epitaxial LiTi_2O_4 thin films were successfully grown by PLD [22,23], thus opening the door for systematic experiments on LiTi_2O_4 and for thin films effects investigation. Indeed, results from charge transport and tunneling spectra on LiTi_2O_4 thin films have shown an anomalous magnetoresistance [24].

In this paper we report angle resolved x-ray photoelectron spectroscopy (AR-XPS) measurements on high quality epitaxial LiTi_2O_4 thin films. The aim of this work is to investigate the surface chemical cation composition, as high quality surface layers are needed to integrate LiTi_2O_4 in full-oxide spin-filtering devices.

2. Experimental details

A $\text{Li}_4\text{Ti}_5\text{O}_{12}$ ceramic target was prepared from a mixture of Li_2CO_3 (Alfa-Aesar) and TiO_2 (Alfa-Aesar) by a standard solid-state reaction method [25]. The higher Li/Ti ratio (0.8) of the target was designed to compensate for the high loss of Li during ablation process [26]. LiTi_2O_4 thin films were grown by PLD (KrF excimer laser, $\lambda=248$ nm) on MgAl_2O_4 (111) (CrysTec GmbH) substrates in vacuum (base pressure 10^{-6} Torr), with a laser fluence of 0.7 J/cm² and a repetition rate of 5 Hz. The substrate temperature was kept at 800 °C during growth (unless stated otherwise) and cooled down to room temperature in vacuum after deposition.

Structural analysis was done using x-ray diffraction (XRD, PANalytical high resolution x-ray diffractometer) with monochromatized $\text{CuK}\alpha_1$ radiation (0.154 nm). Deposition rate was determined by measuring the thickness of ultra-thin films by x-ray reflectivity (XRR) analysis allowing then the controlled deposition of 200 nm-thick films. Due to the closely matched densities of MgAl_2O_4 and LiTi_2O_4 , XRR was performed on films grown on SrTiO_3 (110) (CrysTec GmbH) substrates. Four-point transport measurements were performed between 300 K and 4.2 K by direct Al-bonding to unpatterned films. Atomic force microscopy (AFM) was used to characterize the surface morphology of the films.

AR-XPS measurements (Monochromatized Al-K α laboratory source (1486.6 eV), with a SPECS Phoibos 100 analyzer) were carried out to identify the surface cation composition of the thin films. Spectra were calibrated to the binding energy of C 1s at 284.8 eV and were fitted with Voigt functions for Ti^{3+} , Ti^{4+} and Li peaks to reduce the standard residual between the fit and the experimental data, using CasaXPS 2.3.15 software. The same fitting parameters were used for all spectra and a Shirley background was subtracted. For chemical quantification, we used the sensitivity factors 0.0568 and 0.473 for Li 1s and Ti 3s [27], respectively.

3. Results and discussion

To verify epitaxy and bulk phase purity of the LiTi_2O_4 films, we measured out-of-plane XRD patterns (see Fig. 1a). Single phase epitaxial LiTi_2O_4 film growth on MgAl_2O_4 was confirmed since the spectra showed clear (111) and (222) Bragg's reflection peaks of the film and substrate, with the absence of additional peaks. The average out-of-plane lattice parameter obtained from LiTi_2O_4 diffraction peaks position is almost identical to bulk value, $a=(0.8400 \pm 0.0002)$ nm. The high resolution XRD reciprocal space map (RSM), shown in Fig. 1b, of the substrate (531) peak and the film (531) peak indicates that the latter is fully relaxed in-plane.

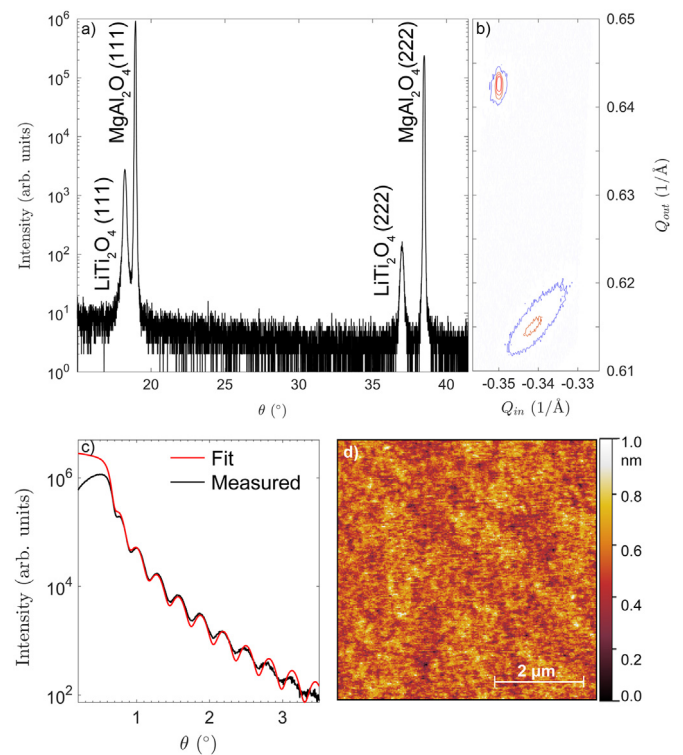


Fig. 1. (a) XRD pattern for the LiTi_2O_4 films around the symmetric (111) MgAl_2O_4 reflection. (b) XRD RSM of the (531) peak of MgAl_2O_4 along with the (531) peak of LiTi_2O_4 . (c) XRR oscillation (black) for a 27 nm LiTi_2O_4 film grown on SrTiO_3 (110) substrate and the simulated fit (red). (d) AFM image of as grown LiTi_2O_4 film. (For interpretation of the references to color in this figure legend, the reader is referred to the web version of this article.)

XRR measurements show Kiessig fringes indicating smooth film surface and thus, a well controlled growth. A reflectivity scan of a 27 nm-thick LiTi_2O_4 film is shown in Fig. 1b, together with the simulated fit. AFM imaging of the films surface (Fig. 1d) confirmed an RMS roughness of 0.4 nm.

As reported by Johnston et al. [19], electrical properties of the $\text{Li}_{1+x}\text{Ti}_{1-x}\text{O}_4$ ternary system depend strongly on the stoichiometry (x). Charge transport characterization on our samples confirmed the high quality thin film growth of the superconducting phase ($x=0$) Li-Ti-O spinel oxide. Fig. 2 shows the metallic behavior at room temperature – $\partial\rho/\partial T > 0$ for $T_c < T < 290$ K – and a sharp normal to superconductor state transition (width < 0.3 K) with a T_c of 13.8 K (inset). The Fermi liquid behavior of the samples resistivity is confirmed by the variation of resistivity as T^2 at lower temperatures (blue line). The residual resistivity ρ_0 and residual resistivity ratio $RRR=\rho_{300\text{K}}/\rho_{15\text{K}}$ of the films were $330 \mu\Omega$ cm and 2.4, respectively, in accordance with the literature [23,24,28,29].

Both XRD and transport measurements strongly indicate that bulk properties of the LiTi_2O_4 films are of very high quality. Film surface composition plays a critical role in tunnel devices, thus XPS measurements were carried out in order to determine the surface composition of the deposited LiTi_2O_4 thin films. Interestingly, the two different spinel phases, LiTi_2O_4 and $\text{Li}_{4/3}\text{Ti}_{5/3}\text{O}_4$, not only have an evident stoichiometric Li to Ti ratio difference, but also the valence state of Ti differs: the average charge of the titanium ions increases from $3.5+$ (an equally mixed valence Ti^{3+} and Ti^{4+}) for superconducting LiTi_2O_4 to $4+$ for insulating $\text{Li}_{4/3}\text{Ti}_{5/3}\text{O}_4$ [30]. XPS is hence a very powerful probing method to differentiate between the two oxides and to get a clear understanding of the chemical composition of the film surface layers. Moreover, the probed depth is almost similar for Li 1s and Ti 3s as their binding energies are close to each other: 55 eV and 62 eV, respectively. In addition, any

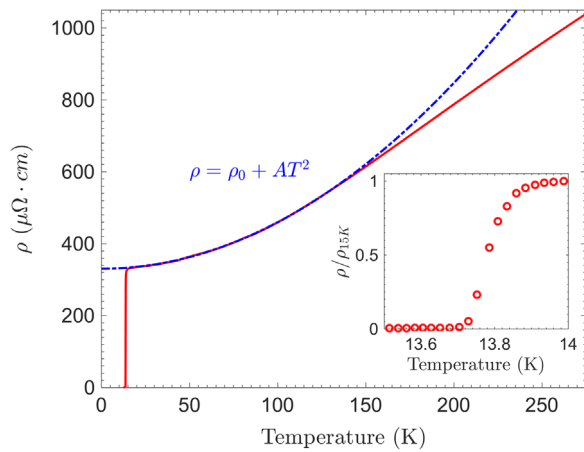


Fig. 2. Temperature dependence of resistivity for LiTi_2O_4 film (red-solid line). Blue-dotted line is the $\rho = \rho_0 + AT^2$ fit in the temperature range 40–120 K. The inset shows the transition from normal to superconducting state. (For interpretation of the references to color in this figure legend, the reader is referred to the web version of this article.)

spurious effect arising from the analyzer transmission can be neglected so that the Li/Ti and $\text{Ti}^{3+}/\text{Ti}^{4+}$ intensity ratios can be considered proportional to the ratio between the concentrations.

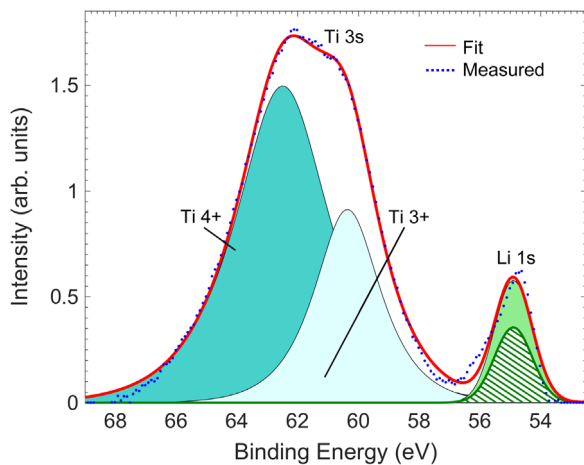


Fig. 3. Measured (dotted-blue) and total fitted (solid-red) Li 1s and Ti 3s XPS bulk-sensitive ($\theta=0^\circ$) spectrum. The areas show the decomposed peak areas for Ti^{4+} (cyan), Ti^{3+} (light cyan) and Li 1s (green). The excess amount of Li present at the surface is clearly visible by comparing the measured Li 1s peak area (green) with the calculated peak area of Li 1s in order to have $\text{Li}/\text{Ti}=0.5$ (hatched green). (For interpretation of the references to color in this figure legend, the reader is referred to the web version of this article.)

Fig. 3 shows experimental XPS data as well as the fits of Li 1s and Ti 3s peaks of the LiTi_2O_4 film at a bulk sensitive emission angle ($\theta=0^\circ$). The Ti 3s peak is clearly split in a Ti^{3+} (~ 60 eV) and a Ti^{4+} (~ 63 eV) component, indicating the presence of LiTi_2O_4 . However, the spectral weight of Ti^{3+} is much less than Ti^{4+} ($\text{Ti}^{4+}/\text{Ti}^{3+} = 2.3$) suggesting that $\text{Li}_{4/3}\text{Ti}_{5/3}\text{O}_4$ is present at the surface.

The formation of $\text{Li}_{4/3}\text{Ti}_{5/3}\text{O}_4$ is also confirmed by an increased Li/Ti ratio of 0.8 compared to 0.5 for LiTi_2O_4 . To enhance clarity of the excess surface concentration of Li (green peak area, **Fig. 3**), the total spectral weight of the Li peak in order to have the correct Li to Ti ratio (0.5), taking into account the total Ti concentration, is depicted in **Fig. 3** by the green-hatched area peak.

To quantify the LiTi_2O_4 cation composition of the surface layers, AR-XPS measurements were performed. Varying the emission angle with respect to the surface normal, allows control of the probing depth, since the effective electron escape depth $\lambda_{\text{eff}} = \lambda \cos \theta$. **Fig. 4**

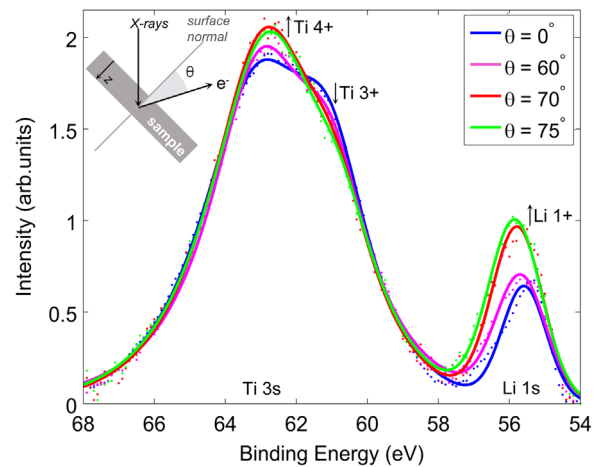


Fig. 4. Measured Li 1s and Ti 3s XPS spectra taken at different collection angles for a LiTi_2O_4 200 nm-thick film grown at 800°C . The arrows indicate the direction of increasing θ . The dots indicate the experimental data, the solid lines are the data envelopes fittings.

shows the Ti 3s, Li 3s spectra and their corresponding total fits – normalized to the Ti 3s area peaks – of LiTi_2O_4 film collected at various emission angles. By increasing θ (i.e. more surface sensitivity) the intensity of the Li 1s peak increases with respect to Ti, clearly indicating a segregation of Li at the LiTi_2O_4 surface. Moreover, the Li 1s peak shape broadens towards higher binding energy, indicating that Li^+ with a different chemical environment is present at the surface. An increase of the Ti^{4+} component with respect to the Ti^{3+} component with increasing θ was present as well.

We calculated the Li to Ti ratio for the different emission angles using the spectral weight of the Ti 3s peak and the spectral weight of the Li 1s peak. The clear increase of Li for larger θ is shown in **Fig. 5a**. Since the Li/Ti intensity ratio is larger than 0.5 and not constant with increasing emission angle, it indicates that the top surface layers are disproportionately Li-rich. Ti^{4+} to Ti^{3+} ratios were calculated from the respective components of the fitted Ti 3s envelopes (**Fig. 5b**). A clear increase of the $\text{Ti}^{4+}/\text{Ti}^{3+}$ ratio was found at higher emission angles, indicating the presence of $\text{Li}_{4/3}\text{Ti}_{5/3}\text{O}_4$ at the top surface layers.

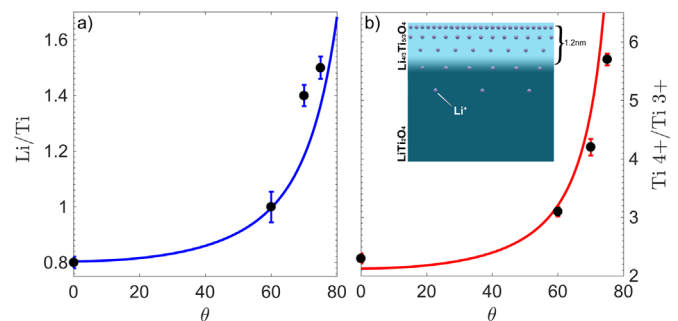


Fig. 5. Measured Li/Ti (a) and $\text{Ti}^{4+}/\text{Ti}^{3+}$ ratios (b) (black dots) for LiTi_2O_4 films. A schematic model of the surface composition used to fit (solid lines) the experimental data is shown in inset b.

To resolve the composition of the surface layers, we modeled the observed Li/Ti and $\text{Ti}^{4+}/\text{Ti}^{3+}$ ratios versus θ . In our model, we took into account that the intensity of the photoelectrons, created at depth z , has a damping factor $\exp(-z/\lambda_{\text{eff}})$, where the electron mean free path (λ) is approximately 2 nm [31]. A surface chemical composition of a mixture of the two different Li-Ti-O spinel compositions, LiTi_2O_4 and $\text{Li}_{4/3}\text{Ti}_{5/3}\text{O}_4$, and of an additional Li phase that mimics the excess of Li at the surface, was hypothesized. Here, the additional Li-phase, modeled by simply using Li^+ ,

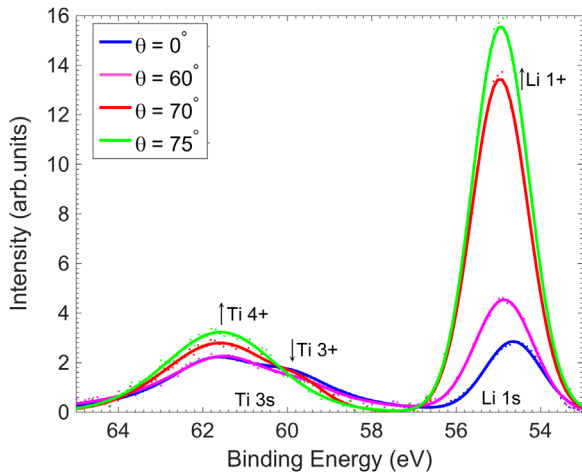


Fig. 6. Measured Li 1s and Ti 3s spectra taken at different collection angles for a LiTi_2O_4 200 nm-thick film grown at 600 °C. The arrows indicate the direction of increasing θ . The dots indicate the experimental data, the solid lines are the data envelopes fitting.

may come from LiCO_3 , LiOH or Li_2O . Note that the presence of Li_2O at the surface could be ruled out, as this phase is accompanied with an O 1s peak at 528.6 eV [32] which was absent in our films (not shown here). With this simple model, we found that a good match (solid lines, Fig. 5) to the experimental data was found if the bulk of the film is LiTi_2O_4 and a thin Li-enriched layer, ~ 1.2 nm (1.5 u.c.), is present at the surface. More precisely, a mixture of Li^+ and $\text{Li}_{4/3}\text{Ti}_{5/3}\text{O}_4$ would be present at the top surface layer and a LiTi_2O_4 – $\text{Li}_{4/3}\text{Ti}_{5/3}\text{O}_4$ mixture towards the bulk. The surface composition is schematically depicted in the inset of Fig. 5b. The presence of a non-spinel Li^{1+} phase at the top surface layer would also clarify the peak broadening of the Li 1s at higher emission angles for increased emission angles.

The Li enrichment at the surface can be understood by considering the increased mobility of Li ions at elevated temperatures as a result of their low activation energy [33]. This leads to an outdiffusion of Li towards the surface that changes the chemical cation compositions of the top LiTi_2O_4 layers. Similar Li-outdiffusion has been observed in e.g. LiNbO_3 crystals [34,35].

To increase the quality of the surface layers, we investigated whether the Li-outdiffusion may be reduced by lowering the growth temperature, even though previous studies have shown that low-temperature growth is detrimental for the quality of LiTi_2O_4 films [29]. By studying the top surface layers of a film grown at 600 °C (with a T_c of 10.7 K) we found that the Li-excess in the surface layers was significantly increased compared to the samples grown at 800 °C. Fig. 6 shows the predominant Li 1s peak with respect to the Ti 3s peak for different collection angles. Here the Li to Ti ratio at $\theta=0^\circ$ was 4.2 ± 0.2 and increased dramatically to 26.5 ± 2.7 for $\theta=75^\circ$. By modeling the data (Fig. 7) using the same procedure used for films grown at 800 °C, we found that for low-temperature growth, the thickness of the Li-excess layer doubles to ~ 2.5 nm. Moreover, Ti would be absent in the top ~ 0.5 nm of the film. The surface composition is schematically depicted in the inset of Fig. 7b.

The increase in Li content at the surface for films grown at lower temperatures is counterintuitive as the outdiffusion may be expected to be reduced. However, previous studies have shown that Li can evaporate from the surface, where the evaporation rate increases with temperature [36,37]. Optimal surface layers are thus obtained when the competing processes of surface segregation and evaporation are balanced, i.e. the thickness of the Li-excess layer has to be kept minimal while keeping the outdiffusion low.

Therefore, we have grown LiTi_2O_4 films in a temperature range of 400–800 °C. The found Li/Ti ratios are shown in inset of Fig. 7a.

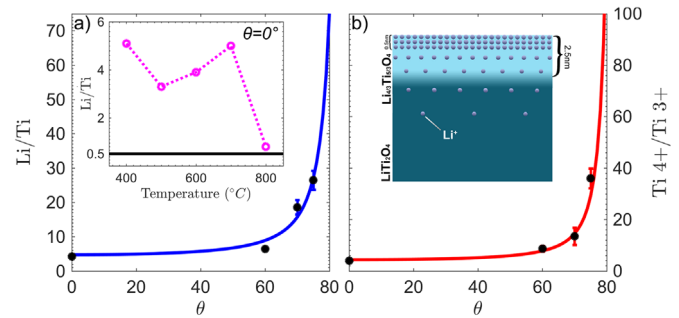


Fig. 7. Measured Li/Ti (a) and $\text{Ti}^{4+}/\text{Ti}^{3+}$ ratios (b) for LiTi_2O_4 films grown at 600 °C (black dots) and the ratios resulting from the best matched model (line). The inset of a shows the Li/Ti ratio (magenta dots) for films grown at different temperatures measured at $\theta=0^\circ$ and the theoretical ratio value of 0.5 (black). The dotted line is a guide to the eye. A schematic model of the surface composition used to fit (solid lines) the experimental data is shown in inset b. (For interpretation of the references to color in this figure legend, the reader is referred to the web version of this article.)

These Li/Ti ratios show that up to 700 °C, the Li excess at the surface is extremely high, suggesting that the Li-evaporation is low. Increasing the growth temperature further, a clear drop in the Li/Ti ratio is present, indicating that Li evaporates from the surface. Taking also the bulk properties into account, our data suggest that a growth temperature of 800 °C is optimal for both high quality LiTi_2O_4 surfaces and bulk properties.

With the presence of Li outdiffusion from bulk to the surface and subsequent Li evaporation, Li-deficiency of the bulk LiTi_2O_4 can be expected. However, since our films grown at 800 °C show a very high T_c , Li-deficiency in the bulk must be very low. Interestingly, a small Li deficiency could also explain our significantly higher T_c (13.8 K) compared to bulk LiTi_2O_4 (11.2 K), which is in agreement with the observations of Capponi et al. [38].

Even though aging effect [39] arising from surface exposure to air contamination during the transfer from PLD to XPS may not be completely ruled out, AR-XPS measurements were also performed on a LiTi_2O_4 film covered by ultra-thin (2 nm) capping layer of CoFe_2O_4 deposited in-situ by PLD directly after the growth of LiTi_2O_4 [40]. The corresponding Li 1s to Ti 3s intensity ratio is very similar to that shown in Fig. 5, suggesting that Li segregation might be an intrinsic phenomenon occurring during growth.

4. Conclusions

We have shown that the growth of metal oxide LiTi_2O_4 thin films by PLD is affected by Li outdiffusion towards the surface. The thickness of the Li-rich layer was found to vary with growth temperature and it is minimized for samples grown at 800 °C, as a result of a balance between Li outdiffusion from bulk and Li evaporation from the surface.

Further analyses are required to ascertain whether the change in chemical composition of the top surface layers affects the formation of APBs, thus hampering formation of a high quality interface with the insulator barrier when the LiTi_2O_4 films are integrated in spin-filter devices. Work is underway to determine the effect of this layer on tunneling process when LiTi_2O_4 is used as electrodes in tunnel junctions.

Acknowledgements

The research leading to these results has received funding from the European Union Seventh Framework Programme ([FP7/2007–2013] [FP7/2007–2011]) under Grant agreement 316657 (Spinlcur),

the European Research Council AdG (291442 “Superspin”), European Research Council AdG (247276 “NOVOX”) and the EPSRC (Equipment Account Grant EP/K035282/1).

References

- [1] J.S. Moodera, T.S. Santos, T. Nagahama, The phenomena of spin-filter tunneling, *J. Phys. Condens. Matter* 19 (2007) 165202, <http://dx.doi.org/10.1088/0953-8984/19/16/165202>.
- [2] M. Julliere, Tunneling between ferromagnetic films, *Phys. Lett. A* 54 (1975) 225–226, [http://dx.doi.org/10.1016/0375-9601\(75\)90174-7](http://dx.doi.org/10.1016/0375-9601(75)90174-7).
- [3] J. Moodera, X. Hao, G. Gibson, R. Meservey, Electron-spin polarization in tunnel junctions in zero applied field with ferromagnetic EuS barriers, *Phys. Rev. Lett.* 61 (1988) 637–640, http://prl.aps.org/abstract/PRL/v61/i5/p637_1.
- [4] J.S. Moodera, R. Meservey, X. Hao, Variation of the electron-spin polarization in EuSe tunnel junctions from zero to near 100% in a magnetic field, *Phys. Rev. Lett.* 70 (1993) 853–856, <http://dx.doi.org/10.1103/PhysRevLett.70.853>.
- [5] T. Santos, J. Moodera, Observation of spin filtering with a ferromagnetic EuO tunnel barrier, *Phys. Rev. B* 69 (2004) 241203, <http://dx.doi.org/10.1103/PhysRevB.69.241203>.
- [6] A. Pal, K. Senapati, Z.H. Barber, M.G. Blamire, Electric-field-dependent spin polarization in GdN spin filter tunnel junctions, *Adv. Mater.* 25 (2013) 5581–5585, <http://dx.doi.org/10.1002/adma.201300636>.
- [7] M. Gajek, M. Bibes, a Barthélémy, K. Bouzehouane, S. Fusil, M. Varela, J. Fontcuberta, a Fert, Spin filtering through ferromagnetic BiMnO₃ tunnel barriers, *Phys. Rev. B* 72 (2005) 020406, <http://dx.doi.org/10.1103/PhysRevB.72.020406>.
- [8] B. Prasad, M. Egilmez, F. Schoofs, T. Fix, M.E. Vickers, W. Zhang, J. Jian, H. Wang, M.G. Blamire, Nanopillar spin filter tunnel junctions with manganite barriers, *Nano Lett.* 14 (2014) 2789–2793, <http://dx.doi.org/10.1021/nl500798b>.
- [9] B. Prasad, W. Zhang, J. Jian, H. Wang, M.G. Blamire, Strongly bias-dependent tunnel magnetoresistance in manganite spin filter tunnel junctions, *Adv. Mater.* 27 (2015) 3079–3084, <http://dx.doi.org/10.1002/adma.201405147>.
- [10] T. Harada, I. Ohkubo, M. Lippmaa, Y. Sakurai, Y. Matsumoto, S. Muto, H. Koinuma, M. Oshima, Spin-filter tunnel junction with matched fermi surfaces, *Phys. Rev. Lett.* 109 (2012) 076602, <http://dx.doi.org/10.1103/PhysRevLett.109.076602>.
- [11] J.-B. Moussy, From epitaxial growth of ferrite thin films to spin-polarized tunnelling, *J. Phys. D Appl. Phys.* 46 (2013) 143001, <http://dx.doi.org/10.1088/0022-3727/46/14/143001>.
- [12] A.V. Ramos, M.-J. Guittet, J.-B. Moussy, R. Mattana, C. Deranlot, F. Petroff, C. Gatel, Room temperature spin filtering in epitaxial cobalt-ferrite tunnel barriers, *Appl. Phys. Lett.* 91 (2007) 122107, <http://dx.doi.org/10.1063/1.2787880>.
- [13] S. Matzen, J.-B. Moussy, R. Mattana, K. Bouzehouane, C. Deranlot, F. Petroff, Nanomagnetism of cobalt ferrite-based spin filters probed by spin-polarized tunneling, *Appl. Phys. Lett.* 101 (2012) 042409, <http://dx.doi.org/10.1063/1.4738790>.
- [14] R. Datta, B. Loukya, N. Li, a Gupta, Structural features of epitaxial NiFe₂O₄ thin films grown on different substrates by direct liquid injection chemical vapor deposition, *J. Cryst. Growth* 345 (2012) 44–50, <http://dx.doi.org/10.1016/j.jcrysgro.2012.02.007>.
- [15] J.X. Ma, D. Mazumdar, G. Kim, H. Sato, N.Z. Bao, A. Gupta, A robust approach for the growth of epitaxial spinel ferrite films, *J. Appl. Phys.* 108 (2010) 063917, <http://dx.doi.org/10.1063/1.3488638>.
- [16] JCPDF-00-040-0407.
- [17] JCPDF-00-005-0672.
- [18] D. Johnston, H. Prakash, W.H. Zachariassen, R. Viswanathan, High temperature superconductivity in the Li-Ti-O ternary system, *Mater. Res. Bull.* 8 (1973) 777–784, [http://dx.doi.org/10.1016/0025-5408\(73\)90183-9](http://dx.doi.org/10.1016/0025-5408(73)90183-9).
- [19] D.C. Johnston, Superconducting and normal state properties of Li_{1+x}Ti_{2-x}O₄ spinel compounds. I. Preparation, crystallography, superconducting properties, electrical resistivity, dielectric behavior, and magnetic susceptibility, *J. Low. Temp. Phys.* 25 (1976) 145–175, <http://dx.doi.org/10.1007/BF00654827>.
- [20] T. Inukai, T. Inamura, N. Telegraph, I. Introduction, Preparation of superconducting LiTi₂O₄ thin films, *Thin Solid Films* 94 (1982) 47–50.
- [21] E. Moshopoulou, Superconductivity in the spinel compound LiTi₂O₄, *J. Am. Ceram. Soc.* 20 (1999) 3317–3320, <http://dx.doi.org/10.1111/j.1151-2916.1999.tb02245.x>.
- [22] R.V. Chopdekar, F.J. Wong, Y. Takamura, E. Arenholz, Y. Suzuki, Growth and characterization of superconducting spinel oxide thin films, *Phys. C Supercond.* 469 (2009) 1885–1891, <http://dx.doi.org/10.1016/j.physc.2009.05.009>.
- [23] A. Kumatani, T. Ohsawa, R. Shimizu, Y. Takagi, S. Shiraki, T. Hitosugi, Growth processes of lithium titanate thin films deposited by using pulsed laser deposition, *Appl. Phys. Lett.* 101 (2012) 123103, <http://dx.doi.org/10.1063/1.4752466>.
- [24] K. Jin, G. He, X. Zhang, S. Maruyama, S. Yasui, R. Suchoski, J. Shin, Y. Jiang, H. S. Yu, J. Yuan, L. Shan, F.V. Kusmartsev, R.L. Greene, I. Takeuchi, Anomalous magnetoresistance in the spinel superconductor LiTi₂O₄, *Nat. Commun.* 6 (2015) 7183, <http://dx.doi.org/10.1038/ncomms8183>.
- [25] M. Hirayama, K. Kim, T. Toujigamori, W. Cho, R. Kanno, Epitaxial growth and electrochemical properties of Li₄Ti₅O₁₂ thin-film lithium battery anodes, *Dalton Trans.* 40 (2011) 2882–2887, <http://dx.doi.org/10.1039/c0dt01477j>.
- [26] T. Dumont, T. Lippert, M. Döbeli, H. Grimmer, J. Ufheil, P. Novák, a Würsig, U. Vogt, a Wokaun, Influence of experimental parameter on the Li-content of LiMn₂O₄ electrodes produced by pulsed laser deposition, *Appl. Surf. Sci.* 252 (2006) 4902–4906, <http://dx.doi.org/10.1016/j.apsusc.2005.07.119>.
- [27] J. Scofield, Hartree-Slater subshell photoionization cross-sections at 1254 and 1487 eV, *J. Electron Spectrosc. Relat. Phenom.* 8 (1976) 129–137, [http://dx.doi.org/10.1016/0368-2048\(76\)80015-1](http://dx.doi.org/10.1016/0368-2048(76)80015-1).
- [28] R. Chopdekar, E. Arenholz, Y. Suzuki, Superconductivity in spinel oxide LiTi₂O₄ epitaxial thin films, *arXiv Prepr. arXiv0707.0522*, 2007, pp. 1–25, <http://arxiv.org/abs/0707.0522>.
- [29] T. Oshima, K. Yokoyama, M. Niwa, A. Ohtomo, Pulsed-laser deposition of superconducting LiTi₂O₄ ultrathin films, *J. Cryst. Growth* 419 (2015) 153–157, <http://dx.doi.org/10.1016/j.jcrysgro.2015.03.029>.
- [30] P. Edwards, R. Egdell, I. Fragala, J.B. Goodenough, M.R. Harrison, A.F. Orchard, E.G. Scott, A study of the spinel materials LiTi₂O₄ and Li₄/3Ti₅/3O₄ by photoelectron spectroscopy, *J. Solid State Chem.* 54 (1984) 127–135, [http://dx.doi.org/10.1016/0022-4596\(84\)90140-3](http://dx.doi.org/10.1016/0022-4596(84)90140-3).
- [31] NIST Standard Reference Database 71, version 2.1.
- [32] K.P.C. Yao, D.G. Kwabi, R. a Quinlan, a N. Mansour, a Grimaud, Y.-L. Lee, Y.-C. Lu, Y. Shao-Horn, Thermal stability of Li₂O₂ and Li₂O for Li-Air batteries: in situ XRD and XPS studies, *J. Electrochem. Soc.* 160 (2013) A824–A831, <http://dx.doi.org/10.1149/2.069306jes>.
- [33] J. Sugiyama, H. Nozaki, I. Umegaki, K. Mukai, K. Miwa, S. Shiraki, T. Hitosugi, A. Suter, T. Prokscha, Z. Salman, J.S. Lord, M. Månsson, Li-ion diffusion in Li₄Ti₅O₁₂ and LiTi₂O₄ battery materials detected by muon spin spectroscopy, *Phys. Rev. B* 92 (2015) 014417, <http://dx.doi.org/10.1103/PhysRevB.92.014417>.
- [34] I.P. Kaminow, Optical waveguiding layers in LiNbO₃ and LiTaO₃, *Appl. Phys. Lett.* 22 (1973) 326, <http://dx.doi.org/10.1063/1.1654657>.
- [35] J.R. Carruthers, I.P. Kaminow, L.W. Stulz, Diffusion kinetics and optical waveguiding properties of outdiffused layers in lithium niobate and lithium tantalate, *Appl. Opt.* 13 (1974) 2333–2342, <http://www.ncbi.nlm.nih.gov/pubmed/20134686>.
- [36] D.L. Hildenbrand, W.F. Hall, N.D. Potter, Thermodynamics of vaporization of lithium oxide, boric oxide, and lithium metaborate, *J. Chem. Phys.* 39 (1963) 296, <http://dx.doi.org/10.1063/1.1734245>.
- [37] Y. Ikeda, H. Ito, G. Matsumoto, S. Nasu, A. Mass, Spectrometric study of vaporization of Li₂O with some refractory metal cells, *J. Mass Spectrom. Soc. Jpn.* 27 (1979) 263–273, <http://dx.doi.org/10.5702/masspec1953.27.263>.
- [38] J.J. Capponi, S. Billat, P. Bordet, B. Lambert-Andron, B. Souletie, Structure, superconducting properties and stoichiometry of Li_{1-x}Ti₂O₄ spinel single crystals, *Phys. C Supercond.* 185–189 (1991) 2721–2722, [http://dx.doi.org/10.1016/0921-4534\(91\)91481-I](http://dx.doi.org/10.1016/0921-4534(91)91481-I).
- [39] T. Inukai, T. Murakami, T. Inamura, Aging effects of Li-Ti-O superconducting compounds, *Jpn. J. Appl. Phys.* 20 (1981) L681–L682, <http://dx.doi.org/10.1143/JJAP.20.L681>.
- [40] S. Mesoraca, M.G. Blamire, 2016. Lithium Titanate and Cobalt Ferrite Spinel Bilayer for Spintronics Applications, in preparation.